Title: Epigenetic programming of host lipid metabolism associates with resistance to TST/IGRA conversion after exposure to *Mycobacterium tuberculosis*

Running title: Host lipid epigenetics and exposure to tuberculosis

Kimberly A Dill-McFarland[a]#, Jason D Simmons[a], Glenna J Peterson[a], Felicia K Nguyen[a], Monica Campo[a]*, Penelope Benchek[b], Catherine M Stein[b,c], Tomas Vaisar[a], Harriet Mayanja-Kizza[d], W Henry Boom[c], Thomas R Hawn[a]

[a] Department of Medicine, University of Washington, Seattle, WA, USA;

[b] Department of Population and Quantitative Health Sciences, Case Western Reserve University, Cleveland, Ohio, USA;

[c] Department of Medicine, Case Western Reserve University, Cleveland, Ohio, USA

[d] Department of Internal Medicine, Makerere University, Kampala, Uganda;

* Current affiliation: Department of Medicine, University of Minnesota, Minneapolis, MN, USA

Correspondence to:

Kimberly A Dill-McFarland

kadm@uw.edu

ABSTRACT

Mycobacterium tuberculosis (Mtb) exposure leads to a range of outcomes including clearance, latent TB infection (LTBI), and pulmonary tuberculosis (TB). Some heavily exposed individuals resist tuberculin skin test (TST) and interferon gamma release assay (IGRA) conversion (RSTR), which suggests that they employ IFNγ-independent mechanisms of Mtb control. Here, we compare monocyte epigenetic profiles of RSTR and LTBI from a Ugandan household contact cohort. Chromatin accessibility did not differ between uninfected RSTR and LTBI monocytes. In contrast, methylation significantly differed at 174 CpG sites and across 63 genomic regions. Consistent with previous transcriptional findings in this cohort, differential methylation was enriched in lipid and cholesterol associated pathways including in the genes APOC3, KCNQ1, and PLA2G3. In addition, methylation was enriched in Hippo signaling, which is associated with cholesterol homeostasis and includes CIT and SHANK2. Lipid export and Hippo signaling pathways were also associated with gene expression in response to Mtb in RSTR as well as IFN stimulation in monocyte-derived macrophages (MDMs) from an independent healthy donor cohort. Moreover, serum-derived HDL from RSTR had elevated ABCA1-mediated cholesterol efflux capacity (CEC) compared to LTBI. Our findings suggest that resistance to TST/IGRA conversion is linked to regulation of lipid accumulation in monocytes, which could facilitate early Mtb clearance among RSTR subjects through IFNγ-independent mechanisms.

IMPORTANCE

Tuberculosis (TB) remains an enduring global health challenge with millions of deaths and new cases each year. Despite recent advances in TB treatment, we lack an effective vaccine or a

durable cure. While heavy exposure to *Mycobacterium tuberculosis* often results in latent TB latent infection (LTBI), subpopulations exist who are either resistant to infection or contain Mtb with IFNγ-independent mechanisms not indicative of LTBI. These resisters provide an opportunity to investigate mechanisms of TB disease and discover novel therapeutic targets. Here, we compare monocyte epigenetic profiles of RSTR and LTBI from a Ugandan household contact cohort. We identify methylation signatures in host lipid and cholesterol pathways with potential relevance to early TB clearance before the sustained IFN responses indicative of LTBI. This adds to a growing body of literature linking TB disease outcomes to host lipids.

INTRODUCTION

Tuberculosis (TB) remains one of the leading causes of single-agent infectious disease death worldwide with over 1 in 1000 people developing new TB and 1.4 million deaths annually (1). Individuals infected with *Mycobacterium tuberculosis* (Mtb), the causative agent of TB, exhibit a range of clinical phenotypes from latent Mtb infection (LTBI) to pulmonary TB disease. LTBI, defined as a positive tuberculin skin test (TST) or interferon (IFN)-γ release assay (IGRA) with no clinical or radiographic evidence of TB disease, describes as much as a quarter of the world's population (2). Some individuals resist TST/IGRA conversion (RSTR) despite prolonged and high-level Mtb exposure (3–6). Many factors likely contribute to resistance to TST/IGRA conversion including genetics, previous *Mycobacterium* infections, lung function, and others (7). We and others previously found differences in immunologic profiles of RSTR and LTBI subjects (5), including transcriptional signatures in monocytes (8, 9). Further investigation of RSTR

63 populations may yield novel insights into host responses to Mtb and identify IFNγ-independent
64 correlates of protection or targets for TB therapeutics.
65
66 Epigenetic mechanisms may regulate transcriptional responses and contribute to RSTR
67 mechanisms. Methylation has been associated with the risk of LTBI conversion (10, 11), anti-
68 mycobacterial activity (12–14), and response to Bacille Calmette-Guérin (BCG), a vaccine for TB
69 disease in children (15). As one of Mtb's first targets in the lung, macrophages are poised to
70 accomplish early Mtb clearance through cell intrinsic microbicidal pathways or by priming IFNγ-
71 independent cellular responses, both of which may operative in the absence of TST/IGRA
72 conversion (16, 17). Some macrophage responses to Mtb infection *in vitro* are modulated
73 through methylation (18), and monocyte responses to BCG have been associated with
74 chromatin remodeling (19). We also previously found that histone deacetylases (HDAC) were
75 differentially expressed in RSTR monocytes compared to LTBI in a Ugandan household contact
76 study (20) and that an HDAC3 inhibitor modulated macrophage signaling during Mtb infection
77 (21). Together, these studies suggest that epigenetic "trained immunity" may regulate Mtb
78 clearance without TST/IGRA conversion.
79
80 In this study, we further characterize immune pathways in a Ugandan RSTR cohort consisting of
81 household contacts of pulmonary TB cases who remain TST/IGRA-negative over 8 - 10 years (3,
82 22). Genome-wide methylation and chromatin accessibility were assessed in unstimulated RSTR
83 and LTBI monocytes. Orthogonal to RSTR transcriptional signatures identified previously (8, 9),

we identify methylation signatures in lipid and cholesterol pathways with potential relevance to IFN responses and macrophage function during Mtb infection.

RESULTS

RSTR methylation differs in lipid and cholesterol associated genes compared to LTBI. We examined chromatin accessibility and methylation in monocytes from RSTR and LTBI individuals (Table 1). RSTR and LTBI groups did not differ by sex, age, body mass index (BMI), BCG vaccination scar, TB exposure score at enrollment (3), or relatedness as measured by total first- and third-degree or closer relationships between each individual and all other individuals in the dataset ($P > 0.05$). All participants were HIV negative.

Epigenetic signals were tested using a linear mixed effects model for RSTR vs LTBI corrected for age, sex, and genetic kinship (Figure S1). Two differentially accessible regions (DAR) and 174 differentially methylated probes (DMP) were identified between RSTR and LTBI at FDR < 0.2 (Figure 1 A,B, Table S1). DMP were then used to define 63 differentially methylated regions (DMR) (FDR < 1E-70) (Figure 1C) each containing two to seven probes (Table S1). In total, 44 of the 63 DMR contained at least one DMP site (Table S1). Significant DAR annotated to one gene (CAMK1D) and an intergenic region. DMP annotated to 125 genes and DMR to 44 genes. Significant epigenetic sites included 40 DMPs and 18 DMRs annotated to promoter regions within 1500 bp of a transcription start site (TSS1500) (Figure S2). Together, these data suggest that RSTR and LTBI monocytes contain distinct epigenetic profiles long after their initial Mtb exposure.

106

107 To assess for connections among the methylation genes, we used hypergeometric mean
108 pathway enrichment analysis with Broad MSigDB gene-sets (23). DMR genes were enriched in
109 11 gene ontology (GO) pathways (FDR < 0.2 and k/K > 0.04, Table S2). No Hallmark gene-sets
110 were significantly enriched, and neither database was enriched within DMP genes. The most
111 highly enriched GO gene-sets for DMR were associated with high-density lipoprotein (HDL)
112 remodeling, lipid export, fatty acid biosynthesis, and Hippo signaling (Figure 2A). Nine DMRs
113 annotated to 8 unique genes (APOC3, CIT, KCNQ1, MCM2, PER3, PLA2G3, RPTOR, SHANK2)
114 drove significant enrichments (Figure 2B, Table S3).

115

116 Among genes enriched in fatty acid, lipid, and HDL pathways (Figure 3A,B), APOC3, KCNQ1, and
117 PLA2G3 each contained one DMR in their TSS1500 region. APOC3 had consistently higher
118 methylation while PLA2G3 had consistently lower methylation as well as a significant DMP site
119 (asterisk) in RSTR compared to LTBI (Figure 3A). In contrast, KCNQ1 had discordant DMR
120 methylation and was driven by a single DMP site with higher methylation in RSTR (asterisk,
121 Figure 3A). Among Hippo signaling associated genes (Figure 3C,D), CIT contained one TSS1500
122 DMR driven by a single DMP site with higher methylation in RSTR compared to LTBI (asterisk,
123 Figure 3C). SHANK2 contained two intronic DMRs both with consistently lower methylation in
124 RSTR compared to LTBI (Figure 3C,D). Together, these data suggest that methylation signatures
125 differentiate RSTR and LTBI monocytes with profiles related to lipid and cholesterol processes.

126

Utilizing a previously published transcriptomics study of this same cohort (9), we next investigated the impacts of Mtb infection on gene expression related to methylation signatures. Among lipid and HDL-associated genes identified in the methylation analysis (Figure 2), APOC3 and PLA2G3 were significantly upregulated while KCNQ1 was downregulated in response to Mtb infection in monocytes (Figure 3E). For Hippo signaling genes, CIT was upregulated and SHANK2 was downregulated after Mtb infection (FDR < 0.05) (Figure 3F). None of these selected genes had differential expression between RSTR and LTBI groups (FDR > 0.2) (Figure 3E,F). Gene-set enrichment analysis (GSEA) further revealed that the lipid export gene-set was upregulated by Mtb infection in both RSTR and LTBI monocytes with the highest expression among Mtb-infected RSTR monocytes (P < 0.05, Figure 4A, Table S4). While GSEA suggested Hippo signaling was not significantly impacted by Mtb infection (FDR > 0.05), RSTR Mtb-infected monocytes had higher Hippo signaling gene expression compared to LTBI (FDR < 0.05, Figure 4A, Table S4). Thus, methylation signatures in uninfected monocytes correlate with Mtb-dependent gene expression patterns that distinguish RSTR from LTBI.

Interferon-specific lipid transcriptional responses in MDM. Given that RSTR and LTBI phenotypes are defined by Mtb-specific IFNγ responses, we next explored IFN-dependent gene expression in pathways associated with methylation. We looked for overlapping enrichment between methylation associated gene-sets described above and the transcriptional responses of an independent healthy cohort's MDMs to Type I and Type II interferons (24). Among the 11 methylation-enriched GO gene-sets, lipid export was significantly up-regulated by IFNα8 stimulation in healthy MDMs (P < 0.05, Figure 4B, Table S4). We then utilized the STRING

protein-protein interaction network to visualize all genes in the GO lipid export gene-set and determine overlap between methylation and transcriptional signatures (Figure 4C). The leading-edge genes for each enrichment analysis were colored to identify genes with differential methylation in RSTR (DMR gene) that likely drive expression changes in RSTR compared to LTBI (RSTR), in response to Mtb infection (Mtb), and/or in response to IFN stimulation (IFNα8, IFNγ, IFN other). As seen in the STRING network (Figure 4C), IFNα8 enrichment was driven by 13 leading-edge genes that mostly overlapped with leading-edge genes in the non-significant interferon stimulations (12/13, Figure 4D). This MDM IFNα8 leading-edge also overlapped with leading-edge genes for lipid export in response to Mtb (8/13) and RSTR compared to LTBI in Mtb infected monocytes (3/13). Together, these data suggest that epigenetic programming may impact lipid export pathways that lead to differences in RSTR and LTBI responses to Mtb infection and may be modulated by IFN induced responses.

In addition, the methylation-enriched Hippo signaling gene-set, which contributes to cholesterol homeostasis (25), was up-regulated by IFNγ ($P < 0.05$, Figure 4B). As visualized in the STRING network (Figure 4D), Hippo signaling in MDMs had 14 leading-edge genes that mostly overlapped with nonsignificant IFN stimulations (12/14) and somewhat overlapped with the RSTR compared to LTBI leading-edge in Mtb infected monocytes (3/13) (Figure 4D). Overall, these data indicate that epigenetically programmed pathways related to Hippo and cholesterol may be impacted by IFNγ induced responses that define RSTR and LTBI phenotypes.

Cholesterol efflux capacity of HDL differs between RSTR and LTBI. To examine lipid-dependent mechanisms of RSTR clearance of Mtb, we next measured serum HDL particle concentrations and sizes as well as cholesterol efflux capacity (CEC) of serum HDL from RSTR and LTBI individuals. Neither HDL particle concentrations nor sizes (xsHDL to xlHDL) differed between unstimulated RSTR and LTBI serum (Figure S3, Table S5, FDR > 0.2). RSTR and LTBI serum HDL had similar total CEC with cAMP activation to stimulate efflux in mouse J774 macrophages (6.1 $\pm$ 1.9 %, P > 0.05, Figure 5A, Table S5). In contrast, ABCA1-specific CEC in BHK cells was higher with RSTR serum HDL compared to LTBI (Δ LTBI = 6.2 $\pm$ 2.1 %, Δ RSTR = 7.5 $\pm$ 2.8 %, P = 0.02) with no differences in unstimulated cells (Figure 5B, Table S5). Moreover, investigation of the previously published transcriptomics study of this same cohort (9) revealed differential expression of ABCA1 in monocytes upon Mtb infection with RSTR displaying significantly higher induction compared to LTBI (Figure 5C). Together, the complimentary effects of increased CEC and ABCA1 may reduce intracellular cholesterol levels during infection and contribute to IFNγ-independent Mtb control in RSTR.

DISCUSSION

We assessed monocyte methylation and chromatin accessibility signatures in latent tuberculosis infection (LTBI) and IGRA/TST resistant individuals (RSTR). We found differential methylation in genes related to high-density lipoprotein (HDL) remodeling, lipid export, and fatty acid metabolism. In addition, ABCA1-mediated HDL cholesterol efflux capacity (CEC) was higher in RSTR compared to LTBI. These results contribute to the growing body of literature

supporting the importance of host lipid and fatty acid metabolism in Mtb infection and disease progression (8, 26).

RSTR had distinct methylation patterns compared to LTBI in genes associated with fatty acid metabolism and lipid transport. These genes included the phospholipase PLA2G3 (27) and lipase repressor APOC3 (28), which associate with HDL and impact intracellular lipid availability. Specifically, an overabundance of APOC3 may reduce HDL-mediated CEC, potentially through competitive binding to the scavenger receptor SCARB1 (29). In addition, the lipid-mediated voltage-gated potassium channel KCNQ1 contained methylation signatures in RSTR. Several KCNQ1 mutations are associated with plasma lipid accumulation (30), and KCNQ1's antisense lncRNA, KCNQ1OT1, is associated with reduced CEC and increased lipid accumulation in macrophages specifically (31). These lipase and lipid transport activities impact free fatty acid (FFA) availability and contribute to the accumulation of lipids. This can lead to lipid-laden, or foamy, macrophages which are a permissive environment for Mtb persistence (32–34). In fact, PLA2G3 directly promotes foamy macrophage accumulation in mice (27). The importance of FFAs in the RSTR phenotype is further supported by previous work in this Ugandan as well as an independent South African cohort, where gene-sets associated with FFA metabolism were more highly expressed in unstimulated RSTR monocytes compared to LTBI (35). Finally, lipid transport after Mtb infection may be further regulated by IFN signaling, a defining feature of RSTR, as indicated by upregulation of lipid export gene expression in response to Mtb infection in RSTR monocytes and to IFNα8 in monocyte-derived macrophages (MDMs). Thus, differences in RSTR methylation in FFA metabolism and lipid transport genes correlate with transcriptional

213 signatures and suggest that epigenetic programming may control lipid accumulation, thus
214 ultimately preventing Mtb persistence.
215
216 The RSTR phenotype may be additionally mediated by cholesterol as indicated by the previously
217 discussed lipid-associated genes (PLA2G3, APOC3, KCNQ1) as well as additional methylation hits
218 related to Hippo signaling (CIT, SHANK2). Cholesterol represents an important fatty acid for Mtb
219 as it is a preferred carbon source (32, 34) and contributes to macrophage responses to Mtb
220 including membrane lipid rafts permissive to Mtb uptake (36), modulation of cellular function,
221 and development of foamy macrophages (32, 33, 37, 38). Hippo signaling is involved in
222 pleiotropic activities related to cell proliferation, differentiation, and survival (25) including in
223 macrophages (39). Among these functions, Hippo signaling regulates cholesterol levels through
224 sterol regulatory element-binding proteins (SREBPs) (25). We previously identified enrichments
225 in IFNγ signaling that discriminated LTBI from RSTR monocytes (8, 9), an expected finding based
226 on categoric IGRA responses (3, 22). Paradoxically, Hippo signaling expression was increased
227 with IFNγ stimulation in healthy MDMs but associated with Mtb-infected RSTR monocytes. This
228 suggests that Hippo signaling is activated among RSTR and may provide protection against Mtb
229 infection in the absence of IFNγ (3, 22). We further investigated RSTR links to cellular
230 cholesterol by measuring CEC. RSTR serum HDL resulted in higher ABCA1-mediated cholesterol
231 efflux compared to LTBI, thus supporting that RSTR are better able to control intracellular
232 cholesterol accumulation. Together, these findings support a hypothesis that Mtb growth is
233 restricted among RSTR monocytes due to enhanced CEC that leads to decreased intracellular

(40) or membrane (36) cholesterol with CEC potentially regulated by ABCA1 and/or Mtb-induced Hippo signaling as a result of specific methylation signatures.

Our study has several limitations. The peripheral blood monocytes investigated in this study represent an important cell population relevant to TB disease. However, epigenetic profiles in lung resident cell populations such as alveolar macrophages may reveal additional markers of the RSTR phenotype. Additionally, while methylation is known to alter gene expression, the impacts of hyper- vs hypomethylation are not clear for gene expression directionality or association with disease (41, 42). Therefore, a more complete analysis of RSTR with paired methylation and gene expression in Mtb-infected cells is needed to elucidate the impacts of methylation on Mtb-relevant gene expression. This design may also reveal differences in chromatin accessibility not captured in the current dataset from uninfected cells. While methylation remains relatively stable over time, changes can occur on the time scale of years to decades (43). This RSTR cohort was defined by long-term follow-up spanning up to 10 years. Thus, the epigenetic markers of this stringently defined RSTR phenotype that was sampled long after documented exposure may not fully capture mechanisms relevant to Mtb clearance at the time of exposure. Finally, these findings are based on a single RSTR cohort, and epigenetic inquiry into additional cohorts with varied RSTR definitions is needed to confirm findings applicable to a larger population.

Overall, these results indicate that RSTR have distinct epigenetic programming related to lipid and cholesterol transport in monocytes. Differentially methylated genes in RSTR and LTBI likely

lead to differences in lipid accumulation in monocytes and this, in turn, may alter Mtb outcomes and contribute to IFNγ independent control of Mtb in RSTR. Together with previous work in this cohort (8, 9, 44), this study supports the role of lipid and fatty acid metabolism in defining the Ugandan RSTR cohort as well as provides novel targets for the development of TB treatment.

METHODS

Cohort. Individuals with culture-positive pulmonary tuberculosis (TB) were recruited as part of the Kawempe Community Health Study in Kampala, Uganda from 2002 to 2012 as previously described (3, 22). Household contacts of index cases were initially followed for 2 years with serial tuberculin skin test (TST) monitoring (22). A subset of individuals were retraced from 2014 and 2017 and re-assessed by TST as well as IFNγ release assays (IGRA) for another 2 years (3). Individuals were classified as concordant negative resisters (RSTR) or concordant positive latent tuberculosis infection (LTBI). All participants were at least 15 years old at the time of retracing, HIV-negative, and gave written, informed consent, approved by the institutional review boards of their associated institution. Cryopreserved peripheral blood mononuclear cells (PBMC) and plasma from a subset of retraced individuals were used here.

Cell culture and DNA extraction. Cryopreserved PBMCs were thawed, washed, and resuspended at 2E6 cells/mL in RPMI-10 supplemented with M-CSF (50 ng/mL), then rested overnight in 6-well non-TC treated dishes. CD14+/CD16+ monocytes were isolated by negative selection magnetic bead column purification (Pan Monocyte Isolation Kit, Miltenyi Biotec). For

chromatin accessibility (ATAC-seq), 5x10E4 monocytes were removed and lysed in resuspension buffer (10 mM Tris-HCl pH 7.4, 10 mM NaCl, 3 mM $MgCl_2$) plus 0.1% NP40, 0.1% Tween-20, and 0.01% digitonin. Cells were lysed on ice for 3 minutes and then washed in resuspension buffer plus 0.1% Tween-20. Nuclei were centrifuged for 10 min at 500xg and 4°C. Supernatant was removed and nuclei were resuspended in 50 µL of transposition mix (Tagment DNA Buffer, 0.1% Tween-20, 0.05% digitonin, 2.5 µL Tagment DNA Enzyme). Transposition reactions were incubated for 30 minutes at 37°C with shaking at 10E3 RPM. DNA fragments were purified with MinElute Reaction kit according to the manufacturer's instructions (Qiagen). For methylation, monocytes were plated at 5x10E5 per well in RPMI-10 supplemented with M-CSF. After 24 hours, media was removed, and genomic DNA was isolated using Quick-gDNA MiniPrep kit according to the manufacturer's instructions (Zymo Research).

Chromatin accessibility. DNA from unstimulated monocytes was amplified by PCR for 5 cycles with indexing primer and barcoded primers. Amplicons were purified with the Agencourt AMPure XP Purification Kit (Beckman Coulter) and sequenced using 50 bp paired-end Tn5 transposase-accessible chromatin sequencing (ATAC-seq) on a NovaSeq6000. Sequence quality was assessed using FastQC (v0.11.8 (45)), and sequencing adapters were removed using AdapterRemoval (v2.3.1 (46)). Reads were aligned to the human genome (GRCh38) using STAR (v2.7.5 (47)), and alignments were assessed with Picard (v2.33.3 (48)) and samtools (v1.10 (49)). Peaks were called from alignments using Genrich (v0.6 (50)) with PCR duplicates removed and using the default ATAC-seq mode. Further data cleaning was completed in R (v4.0.2 (51)). Consensus peaks across samples were determined using ChIPQC (v1.24.1 (52)). Blacklisted

(5421 (53)), mitochondrial (1), and rare peaks (32537 present in < 10% of samples) were removed. Nucleosome-free reads in peaks were quantified with Rsubread (v2.2.4 (54)) and filtered to peaks on autosomal chromosomes with > 0.1 counts per million (CPM) in at least 10% of samples. This resulted in 40919 peaks and 1.3 million ± 1.1 million s.d. reads per sample. Reads were TMM normalized with edgeR (v3.30.3 (55)) and log2 CPM normalized with limma (v3.44.3 (56)). Peaks were annotated to the human genome using ChIPseeker (v1.24.0 (57)) and the UCSC known gene track for GRCh38 (58).

Methylation. DNA from unstimulated monocytes was bisulfate treated using the EZ-96 DNA Methylation kit (Zymo Research). Bisulfite conversion was confirmed by PCR using Universal Methylated Human DNA Standard with hMLH1 Primers (Zymo Research). Converted DNA was then applied to an Illumina Infinium MethylationEPIC850 BeadChip (865918 probes) and sequenced on a NovaSeq6000. Data cleaning and analysis were performed using ChAMP (v2.18.3 (59)) in R (51). Probes were filtered (59)to remove poor-quality (23907), non-CpG (2860), XY chromosome (16424), and SNP adjacent probes (94347). Beta values for the remaining 728380 probes were normalized using functional normalization, chip bias was removed using Combat, and values were log2 transformed to M values. Probes were annotated to the human genome (hg19) within ChAMP and ported to GRCh38 (60).

Kinship. Kinship was determined as previously described (9). Briefly, genotypes were determined using the Illumina MEGA^{EX} array or Infinium OmniExpress BeadChip as previously reported (44). In PLINK2 (61), SNPs present in both arrays were filtered by Hardy-Weinberg

Equilibrium (P < 1x10E-6), minor allele frequency (MAF > 0.05), call rate (> 0.95), and linkage disequilibrium (LD R^2 < 0.1 in 50 bp windows with a 5 bp slide). Pairwise kinship was calculated using the robust King method for identity-by-descent (IBD, SNPRelate v1.22.0 (62)) and a genetic relationship matrix (GRM, GENESIS v2.18.0 (63)) calculated from these 63812 filtered SNPs.

Differential analyses. Differentially methylated probes (DMP) and differentially methylated regions (DMR) were determined in 29 RSTR and 29 LTBI samples with complete methylation and kinship data. Differentially accessible regions (DAR) were determined for 29 RSTR and 31 LTBI with complete chromatin accessibility and kinship data. DMP and DAR were assessed with kimma (v1.4.4 (64)) using a linear mixed effects model of RSTR vs LTBI corrected for age, sex, and kinship. Genetic kinship was included to account for closely related household contacts, and it improved model fit as assessed by sigma (Figure S1A). Sex and age were included as co-variates as they improved model fit for some sites (Figure S1B) and were significant for many sites (Figure S1C,D). Additional co-variates including body mass index (BMI), tuberculosis exposure score (3), and BCG vaccination scar were removed due to missing data, lack of significance, or no improvement in model fit assessed by residual sigma.

DMP model estimates were then used to determine differentially methylation regions (DMR) in DMRcate (v2.2.1 (65)) with settings recommended in (66) (min probes = 2, lambda = 500 bp, scaling = 5). DMR were assessed at FDR < 1E-70, a slight relaxation of DMRcate's default cutoff of 8.16E-85, which was determined based on the rate of DMP within the data set.

Gene enrichment. Epigenetic sites were annotated to hg38 genes based on overlap with intron, exon, untranslated region (UTR), or promoters defined as within 1500 bp of the transcription start site (TSS1500). DAR were annotated using ChIPseeker, DMP using the Infinium hg38 manifest (60), and DMR using DMRcate. Genes were queried for enrichment in Broad MSigDB (23) Hallmark (H) and gene ontology biological process (C5 GO BP) gene-sets using hypergeometric enrichment with SEARchways (v1.0.0). Gene-sets with FDR < 0.2 and > 4% enrichment (k/K) were considered significant. Gene ontology term similarity was visualized by semantic similarity using rrvgo implementing GOSemSim (67). DAR genes were not assessed due to the small number of associated genes.

Gene expression. Previously, Ugandan RSTR and LTBI monocyte gene expression was profiled with and without 6-hour Mtb infection (9). Differentially expressed genes (DEGs) were defined for the Mtb:RSTR interaction term in a model of Mtb*RSTR corrected for age, sex, sequencing batch, and genetic kinship. This original model was used for ABCA1 expression in the present study. Since several methylation genes of interest did not meet the original study's gene expression cutoff (1 CPM in at least 5% of samples), an additional targeted analysis of these genes was performed. Here, all genes with > 0 CPM in at least 1 sample were obtained and log2 counts per million (CPM) were calculated. Genes of interest (APOC3, CIT, KCNQ1, PLA2G3, SHANK2) were modeled using the same interaction model as the original study, and significant genes were defined at Benjamini-Hochberg FDR < 0.2. In addition, targeted gene-set enrichment analysis (GSEA (68)) was performed for the 11 MSigDB gene-sets that were

significantly enriched in methylation genes. Gene-level fold change estimates were extracted from the original linear mixed effects model for the four Mtb:RSTR contrasts (e.g. Mtb vs media in RSTR, RSTR vs LTBI in media, etc). Significant enrichment using GSEA was defined at $P < 0.05$.

Monocyte-derived macrophages (MDM) stimulated with IFN. Additional analyses were performed with a previously published RNA-seq data set of human MDM stimulated with IFNα8, IFNβ, IFNε, or IFNγ (24). Briefly, MDMs isolated from 5 healthy donors were treated with recombinant interferons for 6 hours. Total RNA was extracted and sequenced as described (24). In this study, linear mixed effects model fold change estimates of IFN-stimulated expression vs unstimulated controls were used in GSEA (68) of the 11 MSigDB gene-sets that were significantly enriched in methylation genes. Significant enrichment using GSEA was defined at $P < 0.05$.

Cholesterol efflux capacity. Cholesterol efflux capacity (CEC) was measured in serum from 41 RSTR and 43 LTBI. CEC of serum HDL was quantified using J774 murine macrophages (ATCC) to measure total CEC and baby hamster kidney fibroblast (BHK) cells transfected with a mifepristone inducible ABCA1 transporter to measure ABCA1-specific CEC as previously described (69, 70). In short, serum from RSTR and LTBI was reconstituted from freshly thawed plasma, and polyethylene glycol (20% PEG8000, 2:5 v/v) was added to precipitate apoB-containing (non-HDL) lipoproteins. After centrifugation, supernatants containing HDL (serum HDL) were incubated for 4 hours with unstimulated or stimulated cells labeled with radiolabeled [^{3}H]-cholesterol (71). For J774 macrophages, the cells were stimulated with cAMP

388 to activate the cells including induction of ABCA1 expression. For BHK cells, stimulation was
389 completed with 0.01 µM mifepristone to specifically induce expression of the ABCA1
390 transporter. Thus, the J774 cell model captures overall efflux of cholesterol through multiple
391 pathways, including ABCA1, while the ABCA1-BHK model specifically measures cholesterol
392 efflux through the ABCA1 pathway.
393
394 For both J774 and BHK cells, HDL CEC (percent total cholesterol effluxed from cells to HDL) was
395 determined as the ratio of radio-labeled cholesterol in the media at the end of the incubation
396 relative to the total in the system (media + cell pellet). For BHK cells, ABCA1-specific efflux was
397 calculated as the difference in the percent efflux between stimulated cells more highly
398 expressing ABCA1 versus unstimulated cells. Total CEC and ABCA1-specific CEC were compared
399 in RSTR and LTBI in a linear mixed effects model corrected for age, sex, and BMI using kimma
400 (64). Significance was evaluated at $P < 0.05$.
401
402 **HDL particle concentration and size.** HDL was assessed for the same participants as CEC. Total
403 lipoprotein fraction was separated from plasma proteins by a single step density
404 ultracentrifugation of EDTA plasma as described previously (72, 73). HDL particle concentration
405 and size were quantified by calibrated differential ion mobility analysis on a differential mobility
406 analyzer (DMA) (TSI Inc., MN) as described previously (72, 73). Six HDL subspecies (extra small,
407 small, medium, medium large, large, extra-large) were fitted to the DMA profiles by
408 unsupervised, iterative curve-fitting using Fityk (74). Because DMA directly quantifies the
409 number of particles, areas under the curve fitted for each subspecies were directly converted to

HDL particle concentration using a calibration curve constructed with a protein standard. For total HDL particle concentration, intra-day and inter-day coefficients of variation (CV) were < 10%. For individual species, CV were < 10% with the exception of xsHDL and sHDL (14.8 and 18.5%, respectively). HDL concentration and size were compared in RSTR and LTBI in a linear mixed effects model corrected for age, sex, and BMI using kimma (64). Significance was evaluated at FDR < 0.2.

Data availability. Access to raw epigenetic and transcriptomic data for the Uganda cohort is available through the NCBI database of Genotypes and Phenotypes (dbGaP) Data Browser (https://www.ncbi.nlm.nih.gov/gap/) under accession 002445.v3.p1 but first must be approved by the data access committee (DAC) for the study site (see Supplemental Methods in (9)). Data related to the MDM-IFN experiment are available in the Gene Expression Omnibus (GEO) GSE236156. Scripts for this manuscript are available at https://github.com/hawn-lab/RSTR_epigenetics_public

FUNDING

This study was supported by NIH grants K08AI143926 and T32AI007044 (to JDS), R01AI124348 (to WHB, TRH, CMS, HMK), U01AI115642 (to WHB, TRH, CMS, and HMK), R33AI138272 (to TRH, WHB, HMK, CMS), K24AI137310 (to TRH). Additionally, this work was support by the Bill and Melinda Gates Foundation grant OPP1151836 (to TRH, WHB, CMS and HMK) and Proteomics and Bioinformatics Core of Diabetes Research Center NIH grant P30 DK017047 (to TV).

ACKNOWLEDGEMENTS

We thank the individual study participants of the Kawempe Community Health Study, study coordinators and the clinical and research staff including LaShaunda Malone, Keith Chervenak, Marla Manning, Dr. Alphonse Okwera, Dr. Moses Joloba, Hussein Kisingo, Sophie Nalukwago, Dorcas Lamunu, Deborah Nsamba, Annet Kawuma, Saidah Menya, Joan Nassuna, Joy Beseke, Michael Odie, Henry Kawoya, and Bonnie Thiel.

TABLES

Table 1.

		Chromatin accessibility	RSTR vs LTBI p-value [a]	Methylation	RSTR vs LTBI p-value [a]
Pass-filter donors with kinship	RSTR	29	*NA*	29	*NA*
	LTBI	31		29	
Female, %		46.7	1	50.0	1
Age at enrollment, yrs		16.7 ± 12.2	0.48	17.2 ± 12.6	0.44
Age at sampling, yrs		25.0 ± 11.7	0.40	25.8 ± 12.3	0.32
BMI		22.6 ± 4.4	0.61	22.9 ± 4.3	0.56
BCG scar, %		60.0	0.50	56.9	0.26
HIV+, %		0	*NA*	0	*NA*
TB exposure score at enrollment		6.2 ± 1.2	0.49	6.1 ± 1.2	0.91
Relatedness [b]					
Mean 3° and closer per person		0.13 ± 0.34	0.92	0.10 ± 0.31	0.40
Mean 1° and closer per person		0.63 ± 0.92	0.86	0.55 ± 0.88	0.77

[a] Continuous metrics expressed at mean ± standard deviation (sd) and tested by t-test. Categorical metrics expressed as percentages and tested by Chi-squared. [b] Relatedness was

443 measured as the total number of first-degree relationships (kinship > 0.5) and third-degree or

444 closer relationships (kinship > 0.125) per person, then summarized as mean ± sd across all

445 individuals. BMI: body mass index, BCG: bacille Calmette-Guerin

FIGURE LEGENDS

Figure 1. Monocyte epigenetic sites associated with RSTR vs LTBI. Genome-wide methylation and chromatin accessibility were assessed in unstimulated monocytes. RSTR and LTBI were compared using a mixed effects model corrected for age, sex, and kinship. (A) Differentially accessible chromatin regions (DAR, N = 40,919) were measured using log2 counts per million (CPM) reads in open chromatin peaks. (B) Differentially methylated probes (DMP, N = 728,380) and (C) differentially methylated DMRcate regions (DMR, N = 63) were measured using log2 M values. Significant hits are defined as FDR < 0.2 for DAR and DMP (solid line) or FDR < 1E-70 for DMR (dashed line). This resulted in 2 DAR, 174 DMP, and 63 DMR significantly different between RSTR and LTBI.

Figure 2. Pathways and genes with differentially methylated regions in RSTR and LTBI monocytes. Differentially methylated regions (DMR) were analyzed with hypergeometric mean pathway enrichment analysis with Broad MSigDB gene sets. (A) Gene ontology gene sets significantly enriched in DMR (FDR < 0.2 and k/K > 0.04). Gene sets visualized by semantic similarity in MDS space. Each dot is a gene set with size indicating percent enrichment (k/K * 100) and colors grouping similar terms. (B) DMR genes within significant GO gene sets. Colored boxes indicate presence in gene sets as in (A). Fold changes of probes in differentially methylated regions (DMR) are indicated by + positive for all probes, - negative for all probes, and -/+ variable across probes with the mean region trend in parentheses.

Figure 3. Methylation regions associated with significantly enriched gene sets in RSTR and LTBI monocytes. Genes annotated to differentially methylated regions (DMR, FDR < 1E-70) were assessed for enrichment in gene ontology (GO) gene sets. DMR associated with significantly enriched gene sets (FDR < 0.2) are grouped by (A,B,E) Ss or (C,D,F) Hippo signaling associated genes. The 3 DMR in other enriched pathways (Figure 2B) are not shown. (A,C) Log2 M values for each probe in a DMR are shown with standard deviation error shading for LTBI (orange) and RSTR (purple). Significant individual probes (DMP) are indicated with * (FDR < 0.2). (B,D) DMRs annotated to their nearest gene. Grey arrows indicate full gene transcripts, and black boxes are DMRs. SHANK2 includes DMR 20 and DMR 59 that are too close to be resolved in (D). (E,F) Log2 normalized gene expression in RSTR and LTBI monocytes with and without Mtb infection. FDR indicates the Mtb vs media comparison (FDR < 0.2). No genes were significant for the main effect RSTR vs LTBI or the interaction of Mtb:RSTR (FDR > 0.2).

Figure 4. Mtb and IFN stimulated gene expression in gene sets enriched for RSTR methylation signature. Gene set enrichment analysis (GSEA) was performed for pathways that were significantly enriched for DMR annotated genes (N = 63 genes, Figure 2). Fold change estimates were used from mixed effects models run on one of two RNAseq data sets. (A) GSEA for Mtb and RSTR contrasts. Monocytes from RSTR and LTBI were infected with Mtb for 6 hours, and gene expression was modeled for the interaction of Mtb and RSTR status (Mtb:RSTR) corrected for age, sex, kinship, and sequencing batch. Contrast fold changes were compared for Mtb infection vs media within RSTR or LTBI as well as RSTR vs LTBI within media or Mtb infected groups. Significant enrichment is indicated in red (P < 0.05). (B) GSEA for IFN stimulation. MDMs

from healthy donors were stimulated with type I and II interferons for 6 hrs. Gene expression was modeled for IFN vs media. (C) All genes in the GO gene set "lipid export from cell" are visualized in the STRING protein-protein interaction network. Color indicates leading-edge GSEA and significant DMR genes. Leading-edge genes include +Mtb vs media in RSTR and/or LTBI (Mtb), RSTR vs LTBI in Mtb-infected samples (RSTR), and IFNα8 stimulation vs media (IFNα8). Genes that were leading edge in non-significant IFNβ, IFNε, and IFNγ GSEA are grouped in "IFN other". Genes annotated to a significant DMR are additionally colored (DMR gene). Edge width indicates STRING combined score with only scores > 400 shown. (D) GO "Hippo signaling" gene set genes are similarly represented, except leading-edge genes for IFNγ are colored and non-significant "IFN other" includes IFNα8, IFNβ, and IFNε.

Figure 5. Total and ABCA1-specific cholesterol efflux capacity in RSTR and LTBI. Cholesterol efflux capacity (CEC) was measured in serum-derived HDL from RSTR and LTBI participants. Serum HDL was incubated for 4 hours with unstimulated or stimulated [^{3}H]-cholesterol labeled cells. CEC was calculated as percent cholesterol in media versus total (media + cell pellet). RSTR and LTBI were compared using a linear model corrected for age sex, and body mass index (BMI). (A) Total CEC from J774 cells was measured after exposure to RSTR and LTBI serum HDL. Macrophages were stimulated with cAMP to increase CEC. (B) CEC in ABCA1-transfected BHK cells with RSTR and LTBI HDL. ABCA1-transfected BHK cells were stimulated with media or mifepristone to induce ABCA1 expression. ABCA1-specific CEC was calculated as stimulated (ABCA1 expressing) BHK minus unstimulated. (C) ABCA1 gene expression in monocytes with and without Mtb infection [9]. RSTR and LTBI monocytes were cultured with and without Mtb

511 infection for 6 hrs. Gene expression was modeled for the interaction between Mtb infection

512 and RSTR status (Mtb:RSTR). Significant Mtb:RSTR contrasts are labeled by FDR (FDR < 0.2).

REFERENCES

1. World Health Organization. 2020. Global tuberculosis report. Geneva.
2. Houben RMGJ, Dodd PJ. 2016. The Global Burden of Latent Tuberculosis Infection: A Re-estimation Using Mathematical Modelling. PLoS Med 13:e1002152.
3. Stein CM, Nsereko M, Malone LL, Okware B, Kisingo H, Nalukwago S, Chervenak K, Mayanja-Kizza H, Hawn TR, Boom WH. 2019. Long-term Stability of Resistance to Latent Mycobacterium tuberculosis Infection in Highly Exposed Tuberculosis Household Contacts in Kampala, Uganda. Clin Infect Dis 68:1705–1712.
4. Mave V, Chandrasekaran P, Chavan A, Shivakumar SVBY, Danasekaran K, Paradkar M, Thiruvengadam K, Kinikar A, Murali L, Gaikwad S, Hanna LE, Kulkarni V, Pattabiraman S, Suryavanshi N, Thomas B, Kohli R, Sivaramakrishnan GN, Pradhan N, Bhanu B, Kagal A, Golub J, Gandhi N, Gupte A, Gupte N, Swaminathan S, Gupta A. 2019. Infection free "resisters" among household contacts of adult pulmonary tuberculosis. PLoS One 14:e0218034.
5. Medawar L, Tukiman HM, Mbayo G, Donkor S, Owolabi O, Sutherland JS. 2019. Analysis of cellular and soluble profiles in QuantiFERON nonconverters, converters, and reverters in the Gambia. Immun Inflamm Dis 7:260–270.
6. Verrall AJ, Alisjahbana B, Apriani L, Novianty N, Nurani AC, van Laarhoven A, Ussher JE, Indrati A, Ruslami R, Netea MG, Sharples K, van Crevel R, Hill PC. 2020. Early Clearance of Mycobacterium tuberculosis: The INFECT Case Contact Cohort Study in Indonesia. J Infect Dis 221:1351–1360.
7. Berrington WR, Hawn TR. 2007. Mycobacterium tuberculosis, macrophages, and the innate immune response: does common variation matter? Immunol Rev 219:167–186.
8. Simmons JD, Van PT, Stein CM, Chihota V, Ntshiqa T, Maenetje P, Peterson GJ, Reynolds A, Benchek P, Velen K, Fielding KL, Grant AD, Graustein AD, Nguyen FK, Seshadri C, Gottardo R, Mayanja-Kizza H, Wallis RS, Churchyard G, Boom WH, Hawn TR. 2021. Monocyte metabolic transcriptional programs associate with resistance to tuberculin skin test/interferon-γ release assay conversion. J Clin Invest 131.
9. Simmons JD, Dill-McFarland KA, Stein CM, Van PT, Violet C, Thobani N, Pholo M, Peterson GJ, Penelope B, Mary N, Kavindhran V, Fielding KL, Grant AD, Raphael G, Harriet M-K, Wallis RS, Gavin C, Henry BW, Hawn TR. 2022. Monocyte Transcriptional Responses to Mycobacterium tuberculosis Associate with Resistance to Tuberculin Skin Test and Interferon Gamma Release Assay Conversion. mSphere 7:e00159-22.
10. Karlsson L, Das J, Nilsson M, Tyrén A, Pehrson I, Idh N, Sayyab S, Paues J, Ugarte-Gil C, Méndez-Aranda M, Lerm M. 2021. A differential DNA methylome signature of pulmonary immune cells from individuals converting to latent tuberculosis infection. Sci Rep 11:19418.
11. Pehrson I, Sayyab S, Das J, Idh N, Paues J, Méndez-Aranda M, Ugarte-Gil C, Lerm M. 2022. The spectrum of tuberculosis described as differential DNA methylation patterns in alveolar macrophages and alveolar T cells. Clin Epigenetics 14:175.
12. Verma D, Parasa VR, Raffetseder J, Martis M, Mehta RB, Netea M, Lerm M. 2017. Anti-mycobacterial activity correlates with altered DNA methylation pattern in immune cells from BCG-vaccinated subjects. Sci Rep 7:12305.
13. Kaufmann E, Sanz J, Dunn JL, Khan N, Mendonça LE, Pacis A, Tzelepis F, Pernet E, Dumaine A, Grenier J-C, Mailhot-Léonard F, Ahmed E, Belle J, Besla R, Mazer B, King

IL, Nijnik A, Robbins CS, Barreiro LB, Divangahi M. 2018. BCG Educates Hematopoietic Stem Cells to Generate Protective Innate Immunity against Tuberculosis. Cell 172:176-190.e19.

14. Braian C, Karlsson L, Das J, Lerm M. 2023. Selected β-Glucans Act as Immune-Training Agents by Improving Anti-Mycobacterial Activity in Human Macrophages: A Pilot Study. J Innate Immun 15:751–764.
15. Das J, Verma D, Gustafsson M, Lerm M. 2019. Identification of DNA methylation patterns predisposing for an efficient response to BCG vaccination in healthy BCG-naïve subjects. Epigenetics 14:589–601.
16. Cohen SB, Gern BH, Delahaye JL, Adams KN, Plumlee CR, Winkler JK, Sherman DR, Gerner MY, Urdahl KB. 2018. Alveolar Macrophages Provide an Early Mycobacterium tuberculosis Niche and Initiate Dissemination. Cell Host Microbe2018/08/23. 24:439-446.e4.
17. Simmons JD, Stein CM, Seshadri C, Campo M, Alter G, Fortune S, Schurr E, Wallis RS, Churchyard G, Mayanja-Kizza H, Boom WH, Hawn TR. 2018. Immunological mechanisms of human resistance to persistent Mycobacterium tuberculosis infection. Nat Rev Immunol 18:575–589.
18. Looney M, Lorenc R, Halushka MK, Karakousis PC. 2021. Key Macrophage Responses to Infection With Mycobacterium tuberculosis Are Co-Regulated by microRNAs and DNA Methylation. Front Immunol 12.
19. Arts RJW, Carvalho A, La Rocca C, Palma C, Rodrigues F, Silvestre R, Kleinnijenhuis J, Lachmandas E, Gonçalves LG, Belinha A, Cunha C, Oosting M, Joosten LAB, Matarese G, van Crevel R, Netea MG. 2016. Immunometabolic Pathways in BCG-Induced Trained Immunity. Cell Rep 17:2562–2571.
20. Seshadri C, Sedaghat N, Campo M, Peterson G, Wells RD, Olson GS, Sherman DR, Stein CM, Mayanja-Kizza H, Shojaie A, Boom WH, Hawn TR. 2017. Transcriptional networks are associated with resistance to Mycobacterium tuberculosis infection. PLoS One 12:e0175844.
21. Campo M, Heater S, Peterson GJ, Simmons JD, Skerrett SJ, Mayanja-Kizza H, Stein CM, Boom WH, Hawn TR. 2021. HDAC3 inhibitor RGFP966 controls bacterial growth and modulates macrophage signaling during Mycobacterium tuberculosis infection. Tuberculosis 127.
22. Stein CM, Zalwango S, Malone LL, Thiel B, Mupere E, Nsereko M, Okware B, Kisingo H, Lancioni CL, Bark CM, Whalen CC, Joloba ML, Boom WH, Mayanja-Kizza H. 2018. Resistance and Susceptibility to Mycobacterium tuberculosis Infection and Disease in Tuberculosis Households in Kampala, Uganda. Am J Epidemiol 187:1477–1489.
23. Dolgalev I. 2019. msigdbr: MSigDB Gene Sets for Multiple Organisms in a Tidy Data Format. 7.0.1.
24. Campo M, Dill-McFarland K, Peterson G, Benson B, Skerrett S, Hawn T. 2024. Human alveolar and monocyte-derived human macrophage responses to Mycobacterium tuberculosis. bioRxiv 2024.02.20.581265.
25. Aylon Y, Oren M. 2016. The Hippo pathway, p53 and cholesterol. Cell Cycle 15:2248–2255.
26. Laval T, Chaumont L, Demangel C. 2021. Not too fat to fight: The emerging role of macrophage fatty acid metabolism in immunity to Mycobacterium tuberculosis. Immunol Rev 301:84–97.

27. Sato H, Kato R, Isogai Y, Saka G, Ohtsuki M, Taketomi Y, Yamamoto K, Tsutsumi K, Yamada J, Masuda S, Ishikawa Y, Ishii T, Kobayashi T, Ikeda K, Taguchi R, Hatakeyama S, Hara S, Kudo I, Itabe H, Murakami M. 2008. Analyses of group III secreted phospholipase A2 transgenic mice reveal potential participation of this enzyme in plasma lipoprotein modification, macrophage foam cell formation, and atherosclerosis. J Biol Chem 283:33483–33497.
28. Calkin AC, Tontonoz P. 2012. Transcriptional integration of metabolism by the nuclear sterol-activated receptors LXR and FXR. Nat Rev Mol Cell Biol 13:213–224.
29. Luo M, Liu A, Wang S, Wang T, Hu D, Wu S, Peng D. 2017. ApoCIII enrichment in HDL impairs HDL-mediated cholesterol efflux capacity. Sci Rep 7:2312.
30. Chen X, Yang Y, Li S, Peng Q, Zheng L, Jin L, Wang X. 2012. Several Polymorphisms of KCNQ1 Gene Are Associated with Plasma Lipid Levels in General Chinese Populations. PLoS One 7:e34229-.
31. Yu X-H, Deng W-Y, Chen J-J, Xu X-D, Liu X-X, Chen L, Shi M-W, Liu Q-X, Tao M, Ren K. 2020. LncRNA kcnq1ot1 promotes lipid accumulation and accelerates atherosclerosis via functioning as a ceRNA through the miR-452-3p/HDAC3/ABCA1 axis. Cell Death Dis 11:1043.
32. Peyron P, Vaubourgeix J, Poquet Y, Levillain F, Botanch C, Bardou F, Daffé M, Emile J-F, Marchou B, Cardona P-J, de Chastellier C, Altare F. 2008. Foamy Macrophages from Tuberculous Patients' Granulomas Constitute a Nutrient-Rich Reservoir for M. tuberculosis Persistence. PLoS Pathog 4:e1000204-.
33. Chandra P, Coullon H, Agarwal M, Goss CW, Philips JA. 2022. Macrophage global metabolomics identifies cholestenone as host/pathogen cometabolite present in human Mycobacterium tuberculosis infection. J Clin Invest 132.
34. Pandey AK, Sassetti CM. 2008. Mycobacterial persistence requires the utilization of host cholesterol. Proceedings of the National Academy of Sciences 105:4376–4380.
35. Simmons JD, Van PT, Stein CM, Chihota V, Ntshiqa T, Maenetje P, Peterson GJ, Reynolds A, Benchek P, Velen K, Fielding KL, Grant AD, Graustein AD, Nguyen FK, Seshadri C, Gottardo R, Mayanja-Kizza H, Wallis RS, Churchyard G, Boom WH, Hawn TR. 2021. Monocyte metabolic transcriptional programs associate with resistance to tuberculin skin test/interferon-γ release assay conversion. J Clin Invest 131.
36. Gatfield J, Pieters J. 2000. Essential Role for Cholesterol in Entry of Mycobacteria into Macrophages. Science (1979) 288:1647–1651.
37. Russell DG, Cardona P-J, Kim M-J, Allain S, Altare F. 2009. Foamy macrophages and the progression of the human tuberculosis granuloma. Nat Immunol 10:943–948.
38. Singh V, Jamwal S, Jain R, Verma P, Gokhale R, Rao KVS. 2012. Mycobacterium tuberculosis-Driven Targeted Recalibration of Macrophage Lipid Homeostasis Promotes the Foamy Phenotype. Cell Host Microbe 12:669–681.
39. Liu Y, An Y, Li G, Wang S. 2023. Regulatory mechanism of macrophage polarization based on Hippo pathway. Front Immunol 14.
40. Pawełczyk J, Brzostek A, Minias A, Płociński P, Rumijowska-Galewicz A, Strapagiel D, Zakrzewska-Czerwińska J, Dziadek J. 2021. Cholesterol-dependent transcriptome remodeling reveals new insight into the contribution of cholesterol to Mycobacterium tuberculosis pathogenesis. Sci Rep 11:12396.
41. Mazzone R, Zwergel C, Artico M, Taurone S, Ralli M, Greco A, Mai A. 2019. The emerging role of epigenetics in human autoimmune disorders. Clin Epigenetics 11:34.

650 42. Ehrlich M. 2002. DNA methylation in cancer: too much, but also too little. Oncogene
651 21:5400–5413.
652 43. Talens RP, Christensen K, Putter H, Willemsen G, Christiansen L, Kremer D, Suchiman
653 HED, Slagboom PE, Boomsma DI, Heijmans BT. 2012. Epigenetic variation during the
654 adult lifespan: cross-sectional and longitudinal data on monozygotic twin pairs. Aging
655 Cell 11:694–703.
656 44. McHenry ML, Benchek P, Malone L, Nsereko M, Mayanja-Kizza H, Boom WH,
657 Williams SM, Hawn TR, Stein CM. 2021. Resistance to TST/IGRA conversion in
658 Uganda: Heritability and Genome-Wide Association Study. EBioMedicine 74.
659 45. Andrews S, Krueger F, Segonds-Pichon Anne, Biggins L, Krueger C, Wingett S. 2012.
660 FastQC: A Quality Control Tool for High Throughput Sequence Data. Babraham, UK.
661 46. Schubert M, Lindgreen S, Orlando L. 2016. AdapterRemoval v2: rapid adapter trimming,
662 identification, and read merging. BMC Res Notes 9:88.
663 47. Dobin A, Davis CA, Schlesinger F, Drenkow J, Zaleski C, Jha S, Batut P, Chaisson M,
664 Gingeras TR. 2013. STAR: ultrafast universal RNA-seq aligner.
665 Bioinformatics2012/10/25. 29:15–21.
666 48. Broad Institute. 2019. Picard Toolkit. 2.18.7. Broad Institute, GitHub repository. Broad
667 Institute.
668 49. Li H, Handsaker B, Wysoker A, Fennell T, Ruan J, Homer N, Marth G, Abecasis G,
669 Durbin R, Subgroup 1000 Genome Project Data Processing. 2009. The Sequence
670 Alignment/Map format and SAMtools. Bioinformatics2009/06/08. 25:2078–2079.
671 50. Gaspar JM. 2018. Genrich. 0.6.
672 51. R Core Team. 2023. R: A language and environment for statistical computing. 4.2.1. R
673 Foundation for Statistical Computing, Vienna, Austria.
674 52. Carroll TS, Liang Z, Salama R, Stark R, de Santiago I. 2014. Impact of artifact removal on
675 ChIP quality metrics in ChIP-seq and ChIP-exo data. Front Genet 5:75.
676 53. Amemiya HM, Kundaje A, Boyle AP. 2019. The ENCODE Blacklist: Identification of
677 Problematic Regions of the Genome. Sci Rep 9:9354.
678 54. Liao Y, Smyth GK, Shi W. 2019. The R package Rsubread is easier, faster, cheaper and
679 better for alignment and quantification of RNA sequencing reads. Nucleic Acids Res
680 47:e47–e47.
681 55. Robinson MD, McCarthy DJ, Smyth GK. 2010. edgeR: a Bioconductor package for
682 differential expression analysis of digital gene expression data. Bioinformatics2009/11/11.
683 26:139–140.
684 56. Ritchie ME, Phipson B, Wu D, Hu Y, Law CW, Shi W, Smyth GK. 2015. limma powers
685 differential expression analyses for RNA-sequencing and microarray studies. Nucleic
686 Acids Res 43:e47.
687 57. Yu G, Wang L-G, He Q-Y. 2015. ChIPseeker: an R/Bioconductor package for ChIP peak
688 annotation, comparison and visualization. Bioinformatics 31:2382–2383.
689 58. Kuhn RM, Haussler D, Kent WJ. 2013. The UCSC genome browser and associated tools.
690 Brief Bioinform2012/08/20. 14:144–161.
691 59. Tian Y, Morris TJ, Webster AP, Yang Z, Beck S, Feber A, Teschendorff AE. 2017.
692 ChAMP: updated methylation analysis pipeline for Illumina BeadChips. Bioinformatics
693 33:3982–3984.

694 60. Zhou W, Laird PW, Shen H. 2016. Comprehensive characterization, annotation and
695 innovative use of Infinium DNA methylation BeadChip probes. Nucleic Acids Res
696 45:e22–e22.
697 61. Chang CC, Chow CC, Tellier LCAM, Vattikuti S, Purcell SM, Lee JJ. 2015. Second-
698 generation PLINK: rising to the challenge of larger and richer datasets. Gigascience 4.
699 62. Zheng X, Levine D, Shen J, Gogarten SM, Laurie C, Weir BS. 2012. A high-performance
700 computing toolset for relatedness and principal component analysis of SNP data.
701 Bioinformatics2012/10/11. 28:3326–3328.
702 63. Gogarten SM, Sofer T, Chen H, Yu C, Brody JA, Thornton TA, Rice KM, Conomos MP.
703 2019. Genetic association testing using the GENESIS R/Bioconductor package.
704 Bioinformatics 35:5346–5348.
705 64. Dill-McFarland KA, Mitchell K, Batchu S, Segnitz RM, Benson B, Janczyk T, Cox MS,
706 Mayanja-Kizza H, Boom WH, Benchek P, Stein CM, Hawn TR, Altman MC. 2023.
707 Kimma: flexible linear mixed effects modeling with kinship covariance for RNA-seq data.
708 Bioinformatics 39:btad279.
709 65. Peters TJ, Buckley MJ, Statham AL, Pidsley R, Samaras K, V Lord R, Clark SJ, Molloy
710 PL. 2015. De novo identification of differentially methylated regions in the human
711 genome. Epigenetics Chromatin 8:6.
712 66. Mallik S, Odom GJ, Gao Z, Gomez L, Chen X, Wang L. 2019. An evaluation of
713 supervised methods for identifying differentially methylated regions in Illumina
714 methylation arrays. Brief Bioinform 20:2224–2235.
715 67. Yu G, Li F, Qin Y, Bo X, Wu Y, Wang S. 2010. GOSemSim: an R package for measuring
716 semantic similarity among GO terms and gene products. Bioinformatics 26:976–978.
717 68. Korotkevich G, Sukhov V, Sergushichev A. 2019. Fast gene set enrichment analysis.
718 bioRxiv 60012.
719 69. de la Llera-Moya M, Drazul-Schrader D, Asztalos BF, Cuchel M, Rader DJ, Rothblat GH.
720 2010. The Ability to Promote Efflux Via ABCA1 Determines the Capacity of Serum
721 Specimens With Similar High-Density Lipoprotein Cholesterol to Remove Cholesterol
722 From Macrophages. Arterioscler Thromb Vasc Biol 30:796–801.
723 70. Vaisar T, Gordon JL, Wimberger J, Heinecke JW, Hinderliter AL, Rubinow DR, Girdler
724 SS, Rubinow KB. 2021. Perimenopausal transdermal estradiol replacement reduces serum
725 HDL cholesterol efflux capacity but improves cardiovascular risk factors. J Clin Lipidol
726 15:151-161.e0.
727 71. Ronsein GE, Hutchins PM, Isquith D, Vaisar T, Zhao X-Q, Heinecke JW. 2016. Niacin
728 Therapy Increases High-Density Lipoprotein Particles and Total Cholesterol Efflux
729 Capacity But Not ABCA1-Specific Cholesterol Efflux in Statin-Treated Subjects.
730 Arterioscler Thromb Vasc Biol 36:404–411.
731 72. Hutchins PM, Ronsein GE, Monette JS, Pamir N, Wimberger J, He Y, Anantharamaiah
732 GM, Kim DS, Ranchalis JE, Jarvik GP, Vaisar T, Heinecke JW. 2014. Quantification of
733 HDL Particle Concentration by Calibrated Ion Mobility Analysis. Clin Chem 60:1393–
734 1401.
735 73. Vaisar T, Kanter JE, Wimberger J, Irwin AD, Gauthier J, Wolfson E, Bahnam V, Wu I-H,
736 Shah H, Keenan HA, Greenbaum CJ, King GL, Heinecke JW, Bornfeldt KE. 2019. High
737 Concentration of Medium-Sized HDL Particles and Enrichment in HDL Paraoxonase 1
738 Associate With Protection From Vascular Complications in People With Long-standing
739 Type 1 Diabetes. Diabetes Care 43:178–186.

74. Wojdyr M. 2010. Fityk: a general-purpose peak fitting program. J Appl Crystallogr 43:1126–1128.

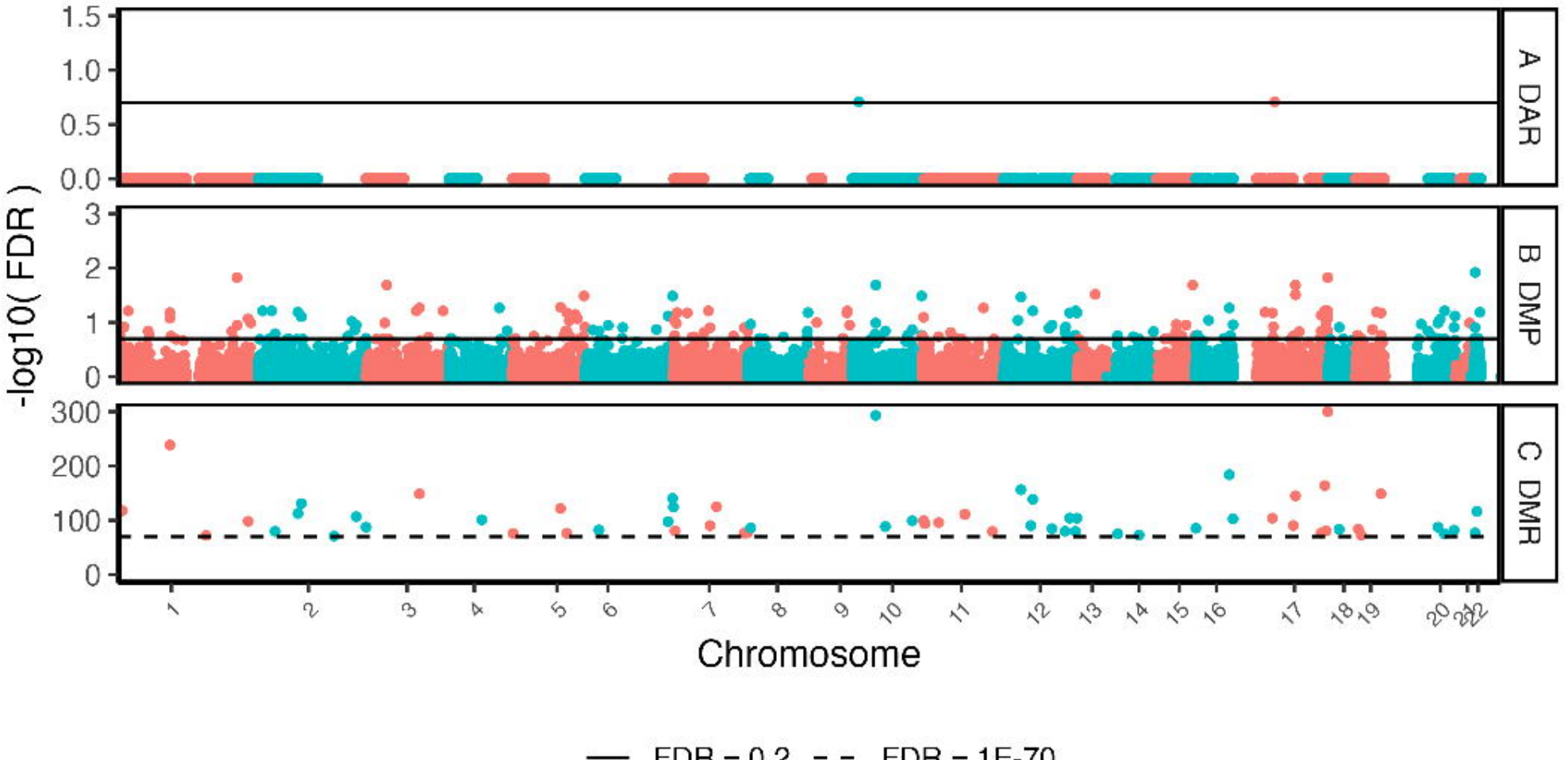
A DAR
B DMP
C DMR
-log10(FDR)
1.5
1.0
0.5
0.0
3
2
1
0
300
200
100
0
1
2
3
4
5
6
7
8
9
10
11
12
13
14
15
16
17
18
19
20
22
Chromosome
FDR = 0.2
FDR = 1E-70

A

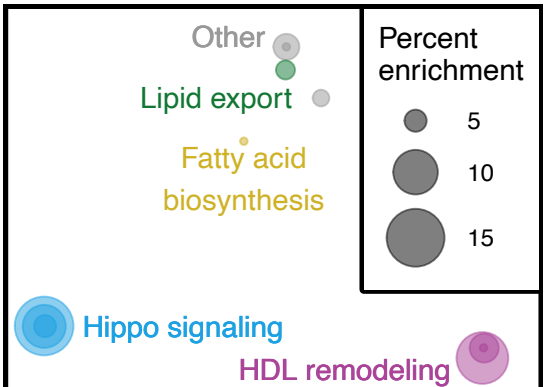

B

Gene	FA	HDL	Hippo	Lipid	Other	Annotation	DMR	Total probes	Log2 M fold change RSTR - LTBI
APOC3						TSS1500	DMR 25	2	+
RPTOR						intron	DMR 18	2	+
PER3						intron	DMR 37	4	-
PLA2G3						TSS1500/5'UTR	DMR 49	5	-
SHANK2						intron	DMR 20	3	-
SHANK2						intron	DMR 59	6	-
CIT						TSS1500/exon	DMR 62	7	-/+ (+)
KCNQ1						TSS1500	DMR 61	6	-/+ (+)
MCM2						intron	DMR 10	2	-/+ (+)

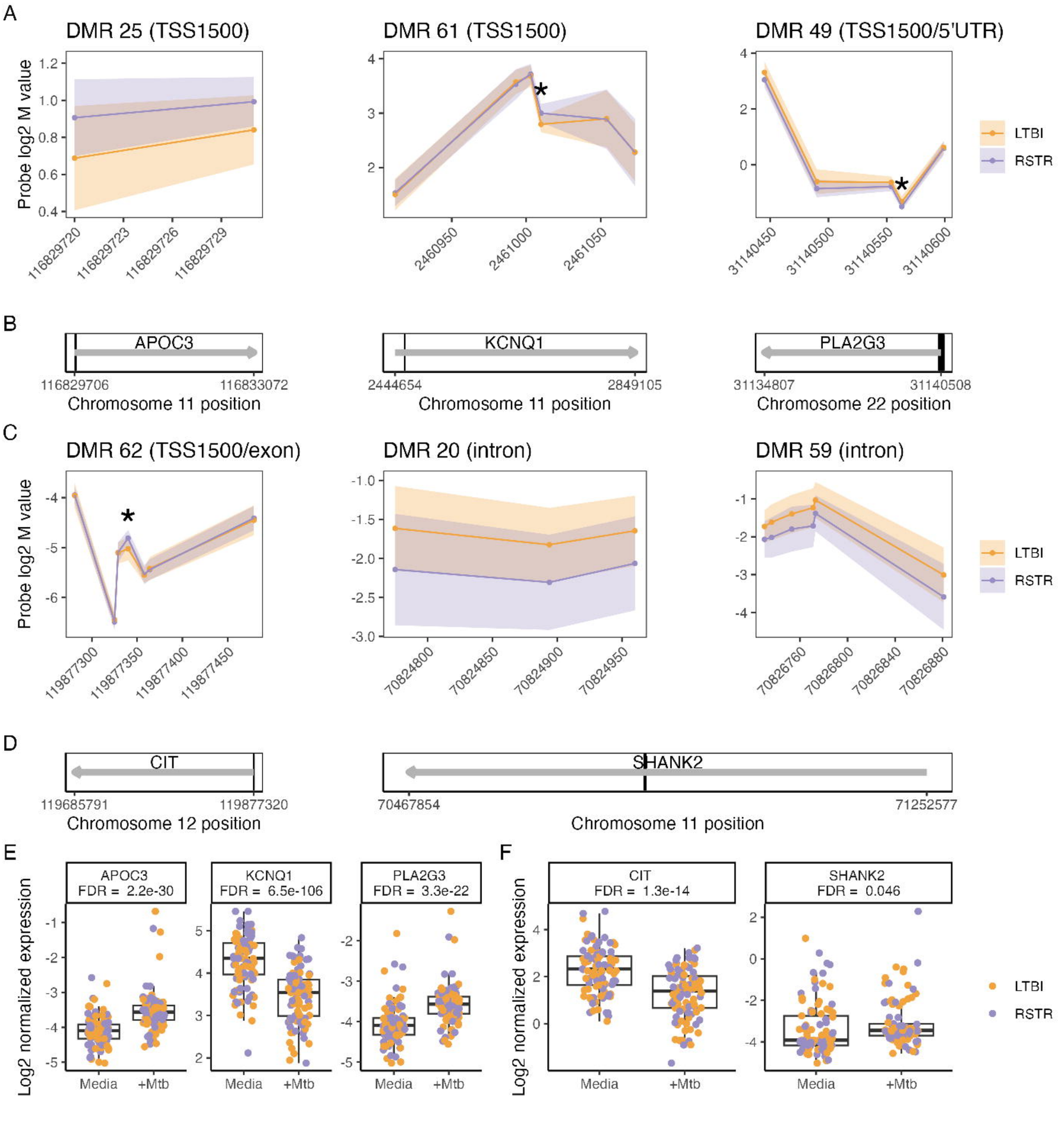
A
DMR 25 (TSS1500)
DMR 61 (TSS1500)
DMR 49 (TSS1500/5'UTR)
Probe log2 M value
LTBI
RSTR
B
APOC3
KCNQ1
PLA2G3
Chromosome 11 position
Chromosome 22 position
C
DMR 62 (TSS1500/exon)
DMR 20 (intron)
DMR 59 (intron)
D
CIT
SHANK2
Chromosome 12 position
Chromosome 11 position
E
APOC3 FDR = 2.2e-30
KCNQ1 FDR = 6.5e-106
PLA2G3 FDR = 3.3e-22
Log2 normalized expression
Media
+Mtb
F
CIT FDR = 1.3e-14
SHANK2 FDR = 0.046

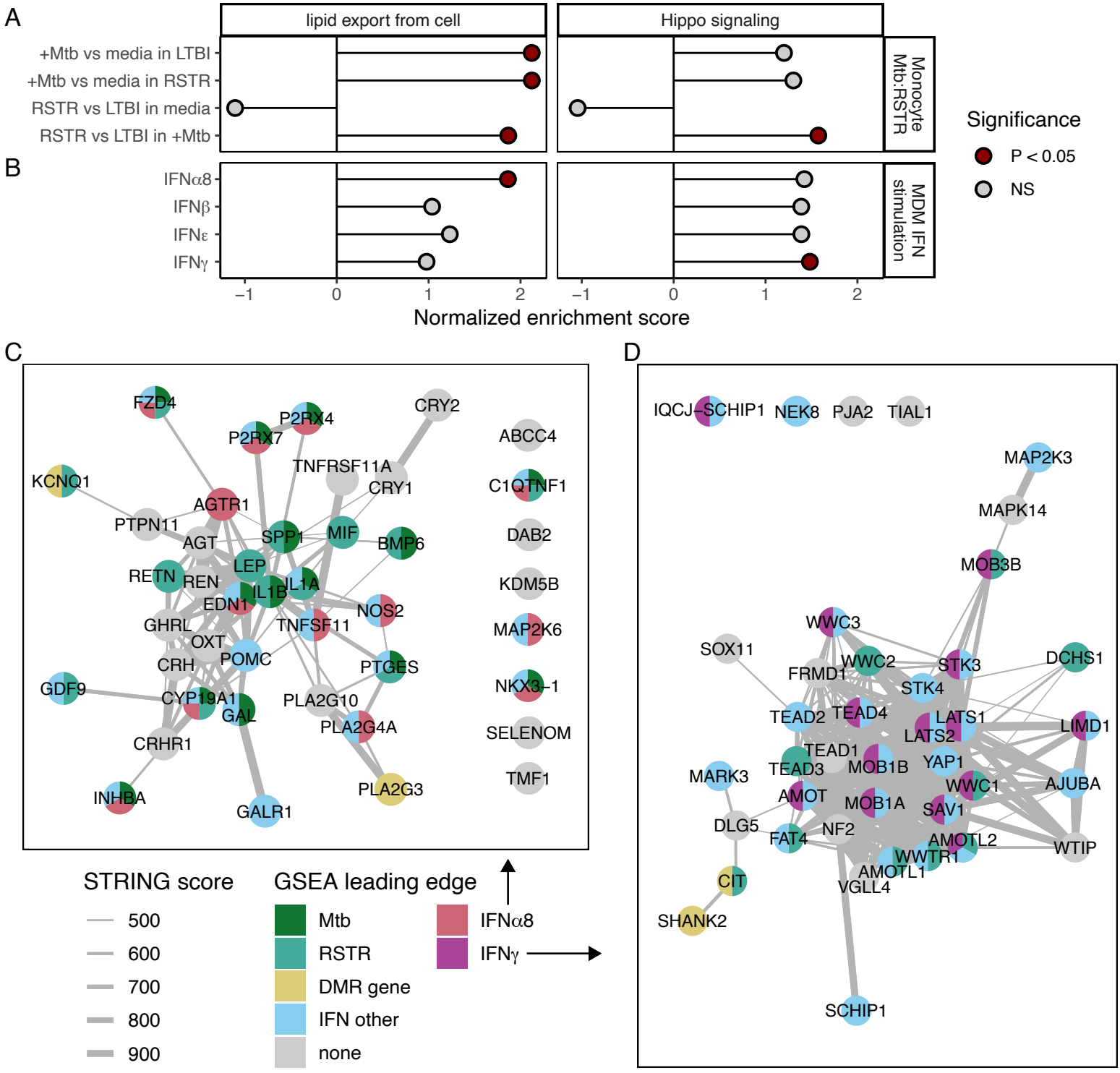
A
lipid export from cell
Hippo signaling
+Mtb vs media in LTBI
+Mtb vs media in RSTR
RSTR vs LTBI in media
RSTR vs LTBI in +Mtb
Monocyte Mtb:RSTR
B
IFNα8
IFNβ
IFNε
IFNγ
MDM IFN stimulation
−1
0
1
2
Normalized enrichment score
Significance
P < 0.05
NS
C
FZD4
P2RX4
P2RX7
CRY2
ABCC4
KCNQ1
TNFRSF11A
CRY1
C1QTNF1
AGTR1
PTPN11
AGT
SPP1
MIF
BMP6
DAB2
RETN
REN
LEP
IL1A
IL1B
KDM5B
EDN1
NOS2
GHRL
TNFSF11
MAP2K6
OXT
CRH
POMC
PTGES
GDF9
CYP19A1
GAL
PLA2G10
NKX3−1
PLA2G4A
SELENOM
CRHR1
INHBA
PLA2G3
TMF1
GALR1
STRING score
500
600
700
800
900
GSEA leading edge
Mtb
RSTR
DMR gene
IFN other
none
IFNα8
IFNγ
D
IQCJ−SCHIP1
NEK8
PJA2
TIAL1
MAP2K3
MAPK14
MOB3B
WWC3
SOX11
WWC2
STK3
DCHS1
FRMD1
STK4
TEAD2
TEAD4
LATS1
LIMD1
LATS2
TEAD1
YAP1
MARK3
TEAD3
MOB1B
WWC1
AJUBA
AMOT
MOB1A
SAV1
DLG5
NF2
FAT4
AMOTL2
WTIP
WWTR1
AMOTL1
CIT
VGLL4
SHANK2
SCHIP1

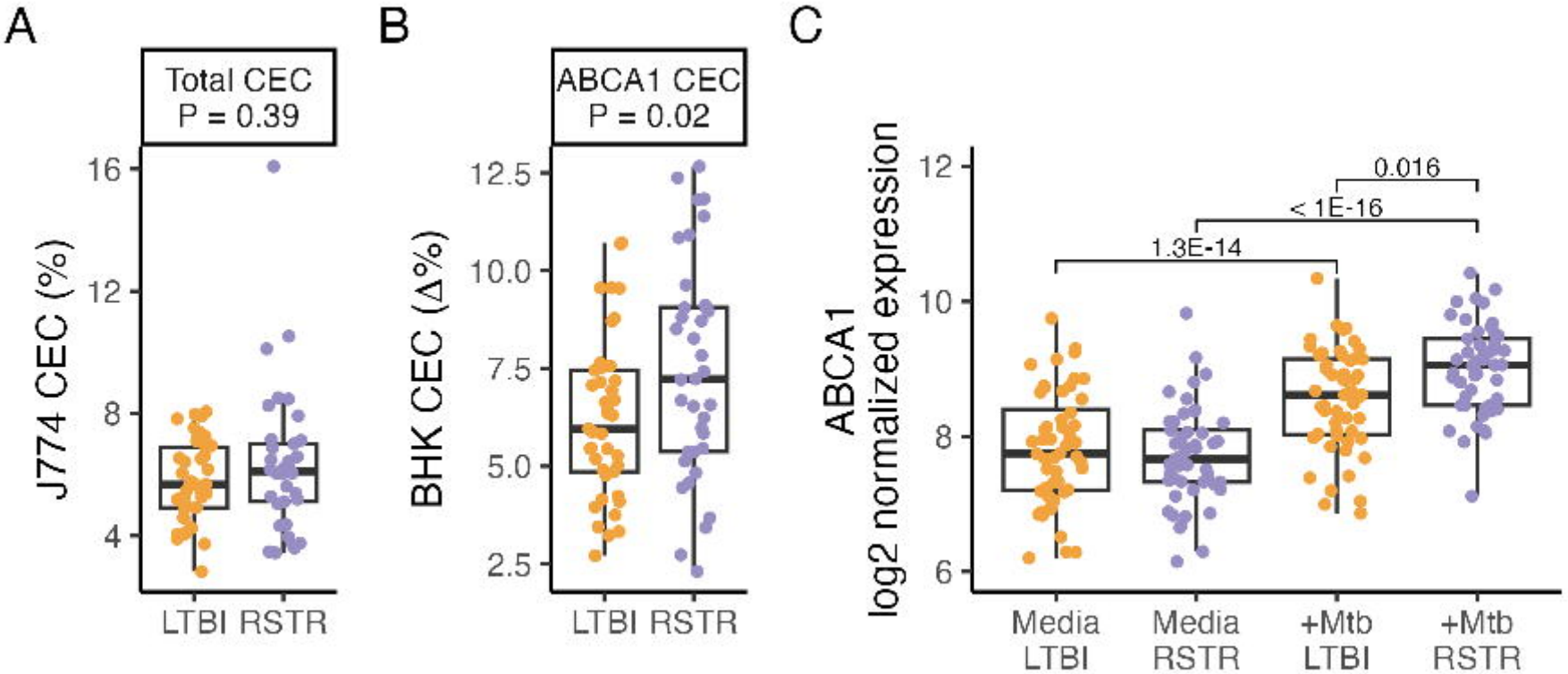
A
Total CEC
P = 0.39
J774 CEC (%)
16
12
8
4
LTBI RSTR
B
ABCA1 CEC
P = 0.02
BHK CEC (Δ%)
12.5
10.0
7.5
5.0
2.5
LTBI RSTR
C
ABCA1
log2 normalized expression
12
10
8
6
0.016
< 1E-16
1.3E-14
Media LTBI
Media RSTR
+Mtb LTBI
+Mtb RSTR